Cellular uptake, cytotoxicity, apoptosis and DNA-binding investigations of Ru(II) complexes

ARTICLE *in* EUROPEAN JOURNAL OF MEDICINAL CHEMISTRY · NOVEMBER 2013

Impact Factor: 3.45 · DOI: 10.1016/j.ejmech.2013.11.005 · Source: PubMed

8 AUTHORS, INCLUDING:

Shobha Devi
National Dong Hwa University
12 PUBLICATIONS **91** CITATIONS
SEE PROFILE

Penumaka Nagababu
Academia Sinica
32 PUBLICATIONS **265** CITATIONS
SEE PROFILE

Sumathi Natarajan
Osmania University
4 PUBLICATIONS **10** CITATIONS
SEE PROFILE

Surya Singh
Osmania University
37 PUBLICATIONS **509** CITATIONS
SEE PROFILE

European Journal of Medicinal Chemistry 72 (2014) 160–169

Contents lists available at ScienceDirect

European Journal of Medicinal Chemistry

journal homepage: http://www.elsevier.com/locate/ejmech

Original article

Cellular uptake, cytotoxicity, apoptosis and DNA-binding investigations of Ru(II) complexes

C. Shobha Devi [a], Penumaka Nagababu [a], Sumathi Natarajan [b], N. Deepika [a], P. Venkat Reddy [a], N. Veerababu [b], Surya S. Singh [b], S. Satyanarayana [a,*]

[a] Department of Chemistry, Osmania University, Hyderabad 500007, Andhra Pradesh, India
[b] Department of Biochemistry, Osmania University, Hyderabad 500007, India

ARTICLE INFO

Article history:
Received 19 August 2013
Accepted 4 November 2013
Available online 25 November 2013

Keywords:
DNA binding
Fluorescence
Cellular uptake
Cytotoxicity
Apoptosis

ABSTRACT

Three new compounds, $[Ru(Hdpa)_2PyIP](ClO_4)_2\cdot 2H_2O$ (**1**) $[Ru(Hdpa)_2FyIP](ClO_4)_2\cdot 2H_2O$ (**2**) and $[Ru(Hdpa)_2IIP](ClO_4)_2\cdot 2H_2O$ (**3**) have been synthesized and characterized by spectroscopic techniques such as elemental analysis, UV/Vis, FT-IR, ^1H NMR, ^{13}C NMR and mass spectra. The CT-DNA binding properties of **1**–**3** have been investigated by absorption, emission spectroscopy and viscosity measurements. Experimental results suggested that they can interact with DNA through intercalative mode with different binding strengths. These were found to promote the cleavage of plasmid DNA. Cell viability results indicated that all compounds showed significant dose dependent cytotoxicity in selected cell lines and **1** shown higher cytotoxicity than cisplatin on HeLa cells. Cellular uptake studies were studied by flow cytometry and confocal microscopy.

1. Introduction

The binding of ruthenium(II) polypyridyl complexes with DNA has been studied extensively since the interaction of these complexes with DNA can cause DNA damage in cancer cells, blocking the division of cancer cells and resulting in cell death. Ruthenium(II) polypyridyl complexes have been used in various fields such as DNA structure probes, chemotherapeutic drugs, molecular light switches, DNA foot printing agents and DNA site specific cleavage [1–4]. These applications are due to the drug-nucleic acid interactions. Stable, inert and water-soluble octahedral complexes containing active metal centers are found to be valuable in the above applications. Octahedral complexes provide useful and sensitive tools for probing DNA structure with site specificity because the complexes can be modified and functionalized in three dimensions to adapt the helix [5].

Both ancillary and intercalative ligands play a crucial role in interaction with DNA [5,6]. The intercalating ligand containing various substituents in different positions can create some interesting properties like electron density distribution, steric hindrance, stability etc., of ruthenium(II) polypyridyl complexes [5,6–8], which will be helpful to more clearly understand the binding mechanism to DNA [9,10]. In recent years many groups have published DNA binding and anticancer activities of ruthenium(II) polypyridyl complexes containing various intercalating ligands [11–13]. Our group also published DNA binding studies on ruthenium(II) polypyridyl complexes containing various ligands [14–18].

To extend this work further, in this paper we report the synthesis and characterization of three new compounds $[Ru(Hdpa)_2PyIP](ClO_4)_2\cdot 2H_2O$ (**1**) $[Ru(Hdpa)_2FyIP](ClO_4)_2\cdot 2H_2O$ (**2**) and $[Ru(Hdpa)_2IIP](ClO_4)_2\cdot 2H_2O$ (**3**) (Hdpa = 2,2′-dipyridylamine), (PyIP = 2-(1-pyrenyl)-1*H*-imidazo[4,5-*f*][1,10]phenanthroline), (FyIP = 2-(2-fluronyl)-1*H*-imidazo[4,5-*f*][1,10-phenanthroline]) and (IIP = 2-(1*H*-Indol-3-yl)-1*H*-imidazo[4,5-*f*][1,10]phenanthroline). Interactions of these compounds with CT-DNA were investigated by UV–visible spectroscopy, fluorescence spectroscopy and viscosity measurement. The *in vitro* cytotoxicity of these compounds was evaluated by MTT assay with various tumor cell lines. Cellular uptake properties on both cancer (HeLa) cell line and normal cells (Lymphocytes isolated from Bovine blood) were studied by flow cytometry and confocal microscopy. Comet assay was done for measuring DNA damage in terms of single and double-strand breaks using HeLa cells to confirm the effects of **1**–**3** on cellular DNA. Molecular docking studies of these compounds were studied by using the GOLD (Genetic Optimization for Ligand Docking) docking program.

* Corresponding author. Tel.: +91 40 2768233.
E-mail address: ssnsirasani@gmail.com (S. Satyanarayana).

0223-5234/$ – see front matter © 2013 Elsevier Masson SAS. All rights reserved.
http://dx.doi.org/10.1016/j.ejmech.2013.11.005

2. Chemistry

2.1. Materials

All reagents and solvents were purchased commercially and used without further purification unless otherwise noted. Ruthenium(III) chloride trihydrate ($RuCl_3 \cdot 3H_2O$) was purchased from (Sigma Aldrich), 1,10-phenanthroline monohydrate and 2,2′-dipyridylamine were purchased from Merck. CT (Calf Thymus) DNA was purchased from Aldrich, Supercoiled pBR322 plasmid DNA (stored at −20 °C) was obtained from Fermentas life sciences, agarose (Genei), MTT and cisplatin (Sigma Aldrich) were used as received. Double distilled water was used for preparing various buffers. Stock solution of cisplatin (5 mM in PBS) was freshly prepared for every experiment.

2.1.1. Analytical measurements

UV–Visible spectra were recorded with an Elico SL159 spectrophotometer. IR spectra were recorded on KBr disks on a Perkin–Elmer FT-IR-1605 spectrometer. ^{1}H NMR spectra were recorded on a Bruker spectrometer with DMSO (D_6) as solvent and tetramethylsilane as an internal standard at 400 MHz at room temperature. Microanalyses (C, H, N) were carried out with a Perkin–Elmer 240 elemental analyzer. Fluorescence measurements were performed on a Hitachi F-2500 spectrofluorimeter. Viscosity experiments were carried out on Ostwald viscometer immersed in thermostated water bath maintained at 30 ± 0.1 °C. Gels were photographed in a Gel doc system (Alpha InfoTech Corporation). Bright Line Heamocytometer (Sigma Ltd.) 96-well plates (Orange Scientific), (Thermo Scientific Multi Skan EX Elisa reader) were used for MTT assay. Flow cytometer (Guava Easycyte 8HT (Millipore)) was used to study cellular uptake and apoptotic inducing activities. Confocal imaging was done by using LeicaTCSSP5 confocal microscope (Leica Microsystems, Wetzlar, Germany) which was equipped with an ArKr laser (used to excite compounds at 488 nm and excitation, at 600–620 nm emission).

3. Results and discussion

3.1. Synthesis and characterization

The ligands PyIP, FyIP and IIP were prepared by the condensation of 1,10-phenanthroline-5,6-dione with respective aldehydes according to the literature methods [19]. The corresponding compounds were synthesized by a direct reaction of $[Ru(Hdpa)_2Cl_2]$ with the appropriate precursor ligands and the desired compounds **1**–**3** (Fig. 1.) were synthesized as their perchlorate salts. A detail description of synthesis and characterization is given in Supporting information (Fig. S1–S6).

The UV–Vis absorption spectra of **1**–**3** showed well resolved bands in the range 200–398 nm characterized by intense π → π* an intra-/interligand transitions. Another band in the visible region, 445–470 (465 nm for **1**, 451 nm for **2** and 447 nm for **3**) was observed, attributed to metal-to-ligand charge transfer (MLCT) Ru dπ → L π* transitions [20]. The infrared spectra of **1**–**3** showed broad band ranges from 3350 to 3050 cm^{-1} represents both N–H and O–H frequency, and (C=N), (C=C) frequencies appeared at around 1625, 1536/1474 (C=C) respectively, which are on the lower frequency side relative to the frequency values obtained for the free ligand indicates the complexation. ^{1}H and ^{13}C[^{1}H] NMR of **1**–**3** resonated in the aromatic region between δ 7.3–9.3 and δ 115–155 which were attributed to the presence of aromatic protons and carbons respectively. In the spectra of **2** a peak at 4.04 δ in ^{1}H NMR and 37.4 δ in ^{13}C[^{1}H] NMR attributed to the presence of $-CH_2$ group. A characteristic peak for the N–H group of the Hdpa ligand is resonated in between 11.00 and 8.91 δ in ^{1}H NMR.

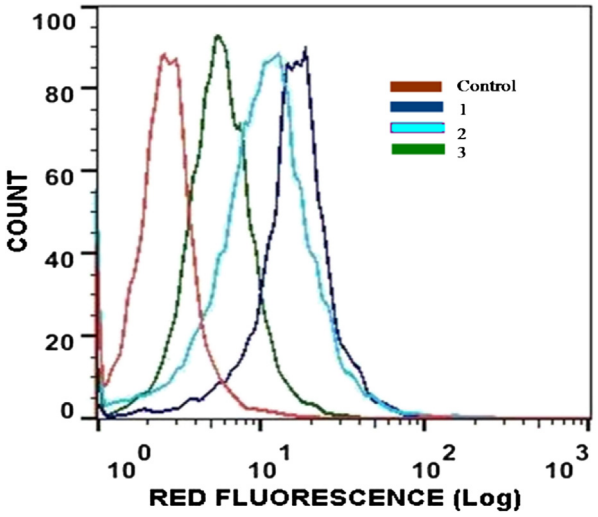

Fig. 2. Flowcytometric results of HeLa cells incubated with untreated cells (control) and **1**–**3** at 37 °C for 1 h. 10,000 events were collected in the FL2 channel.

3.2. Cellular uptake

Flow cytometry and confocal microscopy are suitable techniques for detecting cellular uptake properties of compounds [21–23]. We investigated the cellular uptake and cytotoxic potential of **1**–**3** in HeLa cells and Bovine lymphocytes by using these techniques. The uptake profile of **1**–**3** in HeLa cells incubated with 10 μM concentration for 2 h were given in Fig. 2. The Median-red fluorescence intensity (MFI) values for **1**, **2**, **3** and untreated cells (control), are 16.33, 10.11, 6.28 and 1.1, respectively. These results clearly demonstrated that **1**–**3** have efficient cellular uptake properties in the order **1** > **2** > **3**. These results clearly

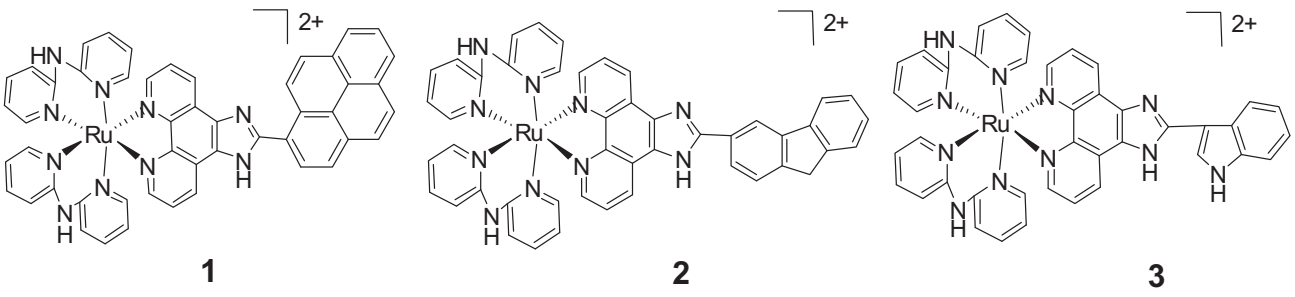

Fig. 1. Structures of complexes **1**–**3**.

demonstrate that they have efficient cellular uptake properties. It has been reported that efficient cellular uptake of compounds are correlated with their lipophilicities [12,24]. The lipophilicities of **1**–**3** in log $P_{o/w}$ are 2.35, 1.23 and 1.11 respectively. The hydrophobicity and larger size of PyIP ligand confer stronger lipophilicity to compound **1**, thereby enhancing its cellular uptake efficiency. A similar phenomenon has also been reported for various ruthenium(II) polypyridyl complexes [23,25,26]. The cellular distribution of **1**–**3** (50 μM) was studied by confocal microscopy. These compounds gradually penetrated into the interior of the nucleus and shown diffuse cytoplasm and nuclear fluorescence after 2 h of incubation with HeLa cells. Control cells exhibit homogeneous nuclear staining, and treated cells display typical changes such as fragmented nuclei or shrinkage indicating DNA cleavage. Confocal images of the control (cells treated with vehicle 1% DMSO) and treated cells (their fluorescent and DAPI stained) are given in Fig. 3.

Cellular uptake properties of **1**–**3** were also studied in normal cells i.e. on lymphocytes. The lymphocytes isolated from bovine blood were incubated with **2** at 50 μM concentration, at different time intervals ranging from 0 to 4 h, the cells were fixed and images acquired by confocal microscopy. These results indicated that the time dependent uptake of compound **2** by lymphocytes. The rate of uptake of compound at 3 and 4 h was more as compared to 1 h. It was clearly observed that the uptake of **2** in normal cells was less than that of HeLa cell line. This implies that the amount of compound **2** taken up by these cancerous cells is greater than that of healthy cells. These results also indicated that the cell membrane was intact even after treatment of **2** with normal cells (lymphocytes), fragmentation in the nucleus or shrinkage was not observed but it was observed in cancerous cells (Fig. 4). This suggests the selectivity of the **2** towards the diseased cells which accounts for a reduction on its general toxicity.

3.3. Apoptosis study

The apoptotic studies were carried out using flow cytometer and the Nexin guava reagent. Different cell types such as viable cells, early apoptotic cells and late apoptotic cells [27] can be distinguished in this apoptosis study using flow cytometer. In the early stages of apoptosis, the cell membrane can expose phosphatidylserine (PS) which is annexin V-positive [28]. The measurement of annexin V binding to the cell surface as an indicator for apoptosis has to be performed along with a dye exclusion test, to establish the integrity of the cell membrane. The HeLa cells were incubated with 10 μM of **1**–**3** for 14 h, followed by staining with Nexin reagent (Annexin V and 7-AAD) and data acquisition by flow cytometer. The percentage of apoptotic cells and changes in DNA content distribution in HeLa cells treated by **1**–**3** were detected by analyzing with Nexin 7-AAD, and Annexin V binding with the help of flow cytometry and Express Pro, FlowJo softwares. Viable cells did not bind to annexin V or 7-AAD (lower left quadrant Q4), early apoptotic cells bound to annexin V but excluded 7-AAD (lower right quadrant Q3), and late apoptotic cells were both annexin V and 7-AAD positive (upper right quadrant Q2). The upper left quadrant Q1 contains dead cells. The results are depicted in Fig. 5. The results indicate that the control cells show 3.59% of late apoptotic cells, whereas number of apoptotic cells increased for all compounds. The order of percentage of apoptotic cells is: **1** > **2** > **3** (**1**, 34.2%; **2**, 19.4% and **3**, 12.9%).

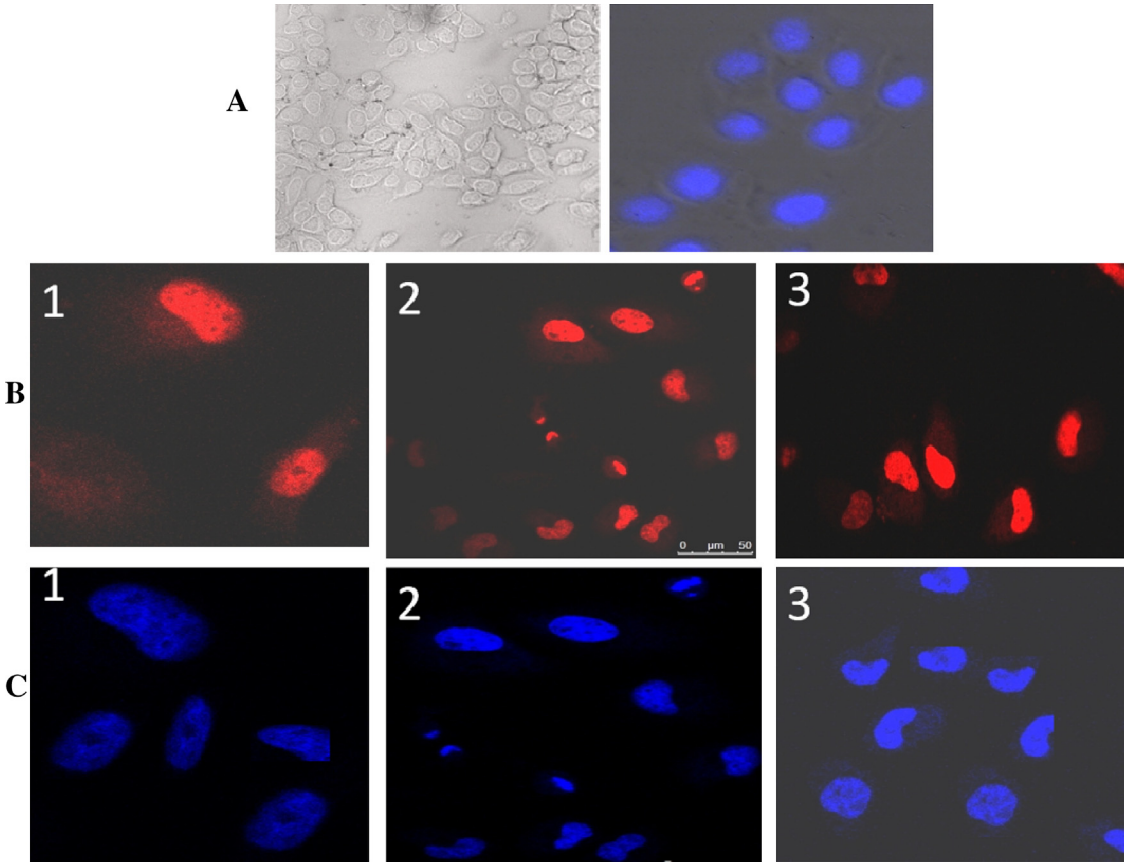

Fig. 3. Confocal images of HeLa cells stained with **1**–**3**. Control (untreated cells) with DAPI stained and fluorescent images (A). Cells were incubated with 50 μM **1**–**3** and observed by confocal microscopy (excitation, 488 nm; emission, 600–620 nm) (B), Cells were incubated with 50 μM **1**–**3** and stained with DAPI (C).

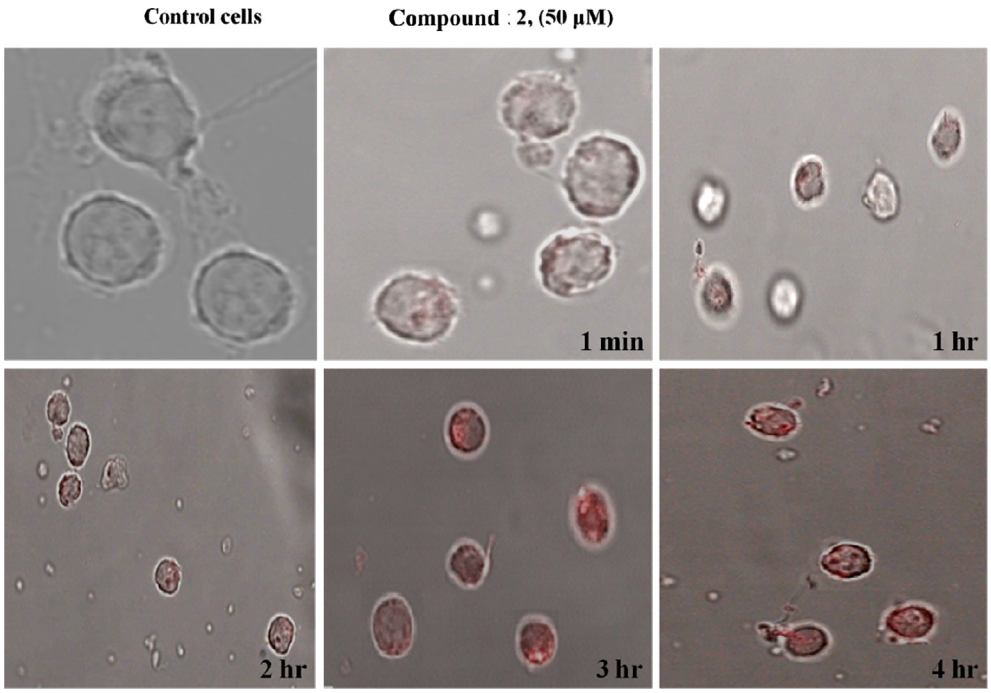

Fig. 4. Confocal images of Lymphocytes treated with compound **2** at different time intervals. Control (untreated cells), cells were incubated with 50 μM compound **2** and observed by confocal microscopy (excitation, 488 nm; emission, 600–620 nm).

3.4. *In vitro cytotoxicity*

The cytotoxicity of **1**–**3** were evaluated on A549 (Human alveolar adenocarcinoma cell line), Du145 (Human Prostate cancer cell lines) and HeLa (Human cervical cancer cell line) by cell survival after 48 h of exposure to **1**–**3** using the MTT assay. They exhibited dose-dependent growth inhibitory effect against the tested cell lines and IC_{50} after 48 h of incubation are given in Table 1. The cell

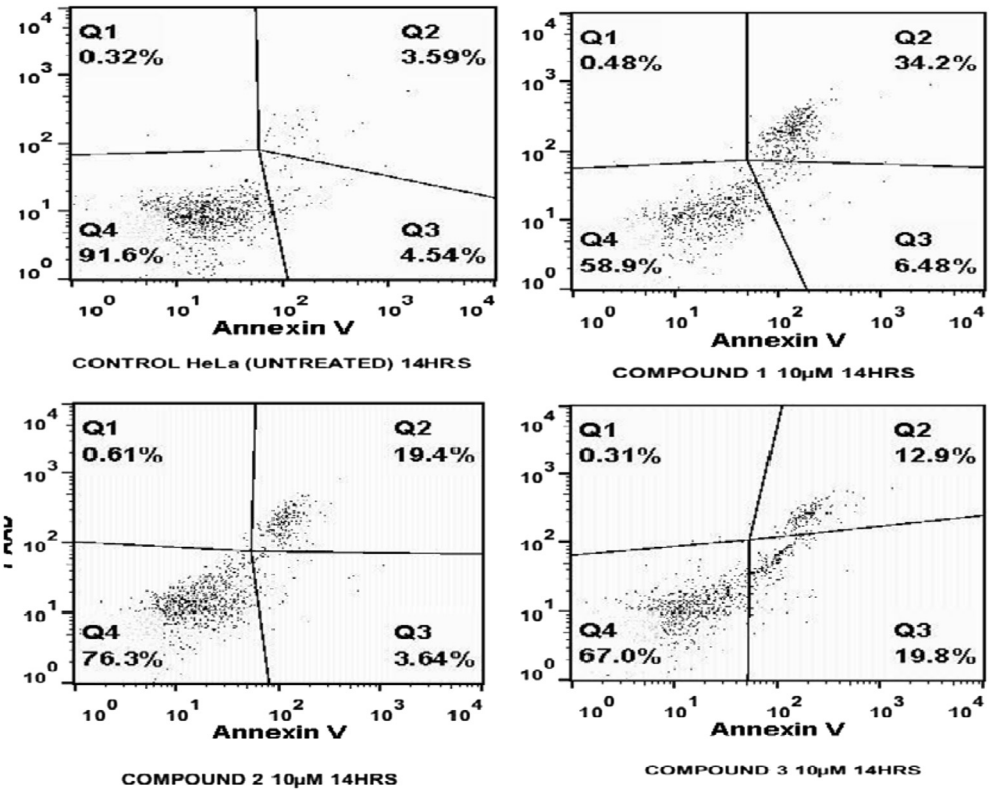

Fig. 5. Nexin (Annexin V and 7-AAD) staining showing differentiated live (Q4), early apoptotic (Q3), late apoptotic (Q2) and dead (Q1) HeLa cells after treatment with **1**–**3** for 14 h. The percents of apoptotic cells were detected by analyzing with flow cytometer using Express Pro and FlowJo softwares.

Table 1
IC_{50} (μM) Values of **1**–**3** and cisplatin against selected cell lines. IC_{50} values are given in μM, cisplatin is included for comparison. Data are presented as mean values ± standard deviations and cell viability assessed after 48 h of incubation.

Complex	A549	Du145	HeLa
1	10 ± 1.2	36 ± 1.4	15 ± 1.2
2	11 ± 0.5	16 ± 0.2	25 ± 0.3
3	43 ± 1.2	35 ± 1.1	32 ± 1.5
Cisplatin	12.3 ± 2.2	6 ± 2.5	19.2 ± 1.2

viability was concentration-dependent (1–100 μM), with increasing the concentrations a decrease in cell viability was observed (Fig. 6). The results shows that **1** has higher activity than remaining, against A549 and HeLa tumor cell lines, and its cytotoxic activity against HeLa cell line was higher than that of cisplatin at comparable conditions. Untreated cells containing the same amount of carrier DMSO were taken as negative control and cisplatin was used as the positive control. The cytotoxicity results are inconsistent with the reported ruthenium(II) polypyridyl complexes [29].

3.5. Emission titration

It was found that the emission intensities for **1**–**3** enhanced on progressive addition of CT-DNA in Tris buffer at ambient temperature, the peaks were found at 588, 591 and 606 nm respectively. This implies that compounds can strongly interact with DNA; the result of compound **3** is given in Fig. 7. The extent of enhancement decreases on moving from **1**–**3**, this indicates strong stacking interaction with DNA. Binding data were cast into the scatchard plot of r/C_f vs r, where r is the binding ratio, C_b/[DNA] and C_f is the free ligand concentration. The K (emission binding constant) values are given in Table 2, the order of the binding constants is **1** > **2** > **3**, indicates that **1** is showing stronger binding ability due to having more planarity in the intercalating ligand.

In order to support the above result, emission quenching experiments were performed using $[Fe(CN)_6]^{4-}$ as quencher. The ferro-cyanide quenching plots for **1**–**3** in the absence, presence and excess of DNA are given in Fig. 8. In the absence of DNA, compounds were efficiently quenched by $[Fe(CN)_6]^{4-}$ resulting in linear Stern–Volmer plots. In excess amount of DNA quenching was less, because

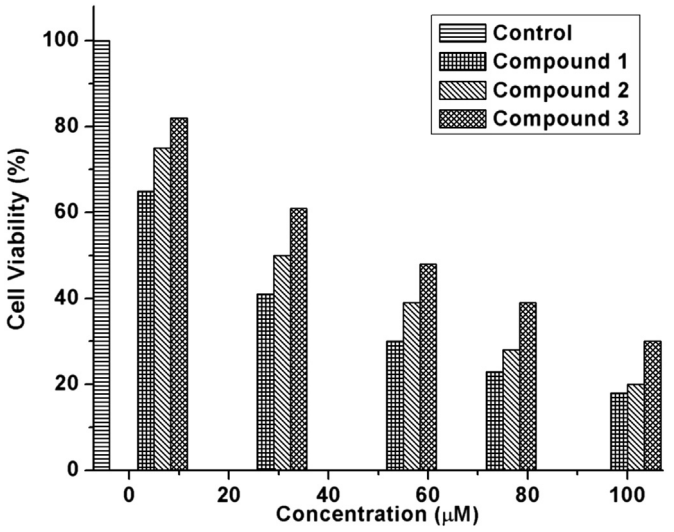

Fig. 6. Cell viability of **1**–**3** on HeLa tumor cells at various concentrations. Untreated cells are used as the control.

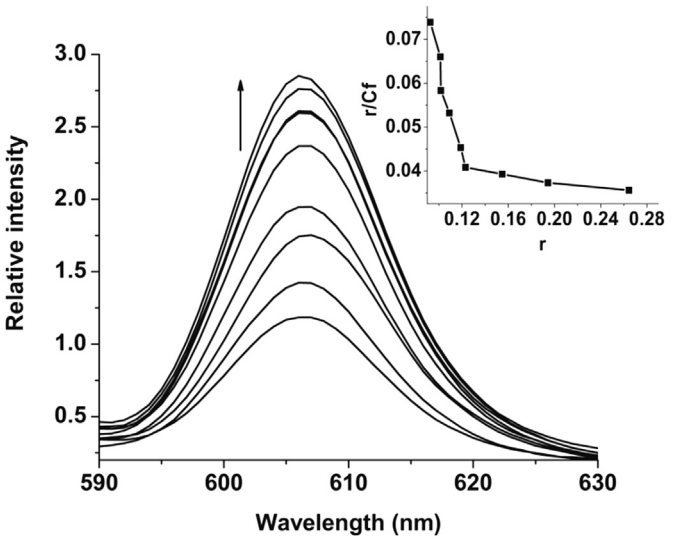

Fig. 7. Emission spectra of **3** in Tris–HCl buffer at 25 °C upon addition of CT-DNA, [Ru] = 20 μM, [DNA] = 0–120 μM. The arrow shows the increase in intensity upon increasing CT-DNA concentrations.

of the highly negatively charged $[Fe(CN)_6]^{4-}$ would be repelled by the negative charge of the DNA phosphate backbone which would hinder the quenching of the emission of the bound compounds. The Stern–Volmer quenching constant K_{sv} can be determined by using Stern–Volmer equation [30].

$$I_0/I = 1 + K_{sv}[Q]$$

where I_0 and I are the fluorescence intensities in the absence and presence of quencher respectively, Q is the concentration of the quencher. In the quenching plot of I_0/I vs [Q], K_{sv} is given by the slope. The quenching constant (K_{sv}) values for **1**–**3**, are given in Table 1.

3.6. Absorption titration

The interactions of **1**–**3** with CT-DNA were investigated using absorption spectroscopy. The titrations were done with varying concentrations of DNA, at constant concentration of the compound, all the absorption bands display clear hypochromism with a concomitant minor red shift. The absorption spectra of **1** in the absence and presence of CT-DNA at constant concentration is given in Fig. 9. These spectral characteristics suggested that they can interact with DNA most likely through a mode that involves a stacking interaction between the aromatic chromophore and the base pairs of DNA. In order to compare the DNA binding affinities quantitatively, their intrinsic binding constant K_b was obtained by monitoring the changes in absorbance at 398, 272 and 302 nm for **1**, **2** and **3** respectively with increasing concentration of DNA. Binding constant values for **1**–**3** are given in Table 1. The binding constants calculated are also in consistent with emission and quenching data. The difference in binding constants may be attributed to their intercalating ligand. This data indicates that the size and the shape of the intercalated ligand has a significant effect on the strength of DNA binding and the most suitable intercalating ligand leads to the highest affinity with DNA. As PyIP possesses greater planar area and extended π system, it penetrates more deeply into DNA base pairs. Hence PyIP has higher hypochromicity than that of FyIP and IIP, therefore binding constant for **1** is higher compared to **2** and **3**. The K_b values are in the same order as those reported earlier for various analogous metallo intercalators [31].

Table 2
Absorption peaks, absorption, emission and quenching binding constants of **1**–**3**.

Compounds	Hypo-chromism	Absorption binding constant K_b (M^{-1})	Emission binding constant (K)	K_{sv} only complex	Compound + DNA	
					1:50	1:200
1	16.4%	8.24×10^5	8.12×10^5	912	585	135
2	17.3%	6.17×10^5	6.25×10^5	667	254	68
3	13.2%	3.41×10^4	3.32×10^4	225	70	17

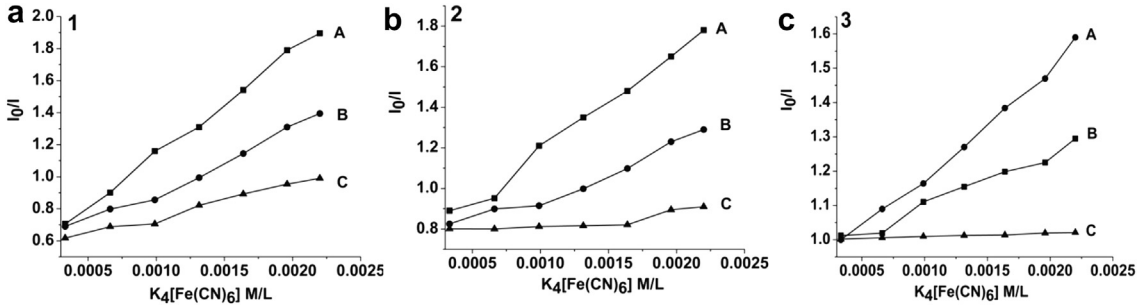

Fig. 8. Emission quenching of **1**–**3** with $K_4[Fe(CN)_6]$ in the absence (a) and presence (b) [Ru] = 20 μM and excess of DNA (c).

3.7. Viscosity

Generally, in absence of any crystallographic structural data, hydrodynamic measurements (such as viscosity, sedimentation, etc.) are the most sensitive techniques to determine DNA binding modes [32]. For further establishment of the interactions between the **1**–**3** and DNA, viscosity measurements were carried out. The relative viscosity of CT-DNA is well known to increase on interaction with intercalative binding substrates. This is because insertion of intercalator causes the base pairs of DNA to separate and thus cause lengthening of the DNA helix. In the presence of compound with DNA viscosity has been found to increase suggesting that they could bind to DNA through intercalation binding mode (Fig. 10). The intercalating strength is in similar order to the above absorption and fluorescence spectroscopic results. All these studies suggest that **1**–**3** have a strong interaction with DNA and the order of affinity is **1** > **2** > **3**.

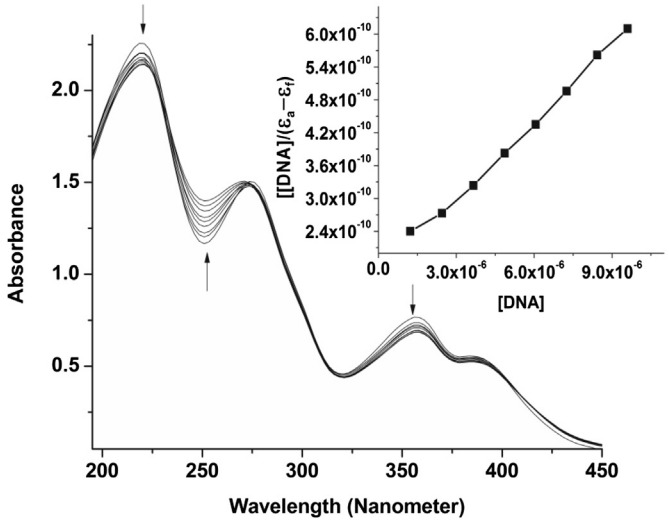

Fig. 9. Absorption spectra of, **1** in tris–HCl buffer upon addition of CT-DNA in absence (*top*) and presence of CT-DNA (*lower*) the [compound] = 10–15 μM [DNA] = 0–120 μM. *Inset* plots of [DNA]/($\varepsilon_a - \varepsilon_f$) versus [DNA] for the titration of DNA with the compound. *Arrow* shows change in absorption with increasing DNA concentration.

3.8. pBR322 DNA cleavage

Gel electrophoresis experiments using pBR322 DNA were performed with **1**–**3** with varying the concentrations, in the presence and absence of Histidine (as singlet oxygen quencher), the efficient cleavage was observed with increase in the concentration. No DNA cleavage was observed for control (unirradiated plasmid DNA) in which compound was absent (lane 0). When plasmid DNA was subjected to electrophoresis, relatively fast migration was observed for the supercoiled form (form I). Cleavage of supercoiled, form I, through single nicking produces open circular DNA (form II), while double nicking produced the linear form (form III), form III migrates in between form I and form II [33]. The intermediacy of singlet molecular oxygen in the photosensitized DNA cleavage with different ruthenium(II) complexes has been put forward in many previous studies [34] and our results are also inconsistent with them. No cleavage was observed in lanes 4, 8 and 12 (Fig. 11), in which compounds treated with pBR322 DNA in presence of histidine.

3.9. Comet assay

Comet assay [35], a versatile and sensitive method for measuring DNA damage in terms of single and double-strand breaks in DNA; was performed using HeLa cells to confirm the effects of the **1**–**3** compounds on cellular DNA. From Fig. 12 it is clear that the compounds causing DNA break down as evidenced by the increase in comet tail length. Also indicates that the DNA damage is seen when HeLa cells are treated with compounds and no damage is seen in control cells which are not treated with compound. The assay on HeLa cells confirms that the DNA damaging was increased with increase in time. The compounds showed DNA damage in the order of **1** > **2** > **3** with comet tails measuring approximately 58 μm, 52 μm and 35 μm for **1**–**3** respectively after 6 h treatment. Time dependent effect of 50 μM of **1**–**3** on DNA integrity of HeLa cells is given in (Fig. S9).

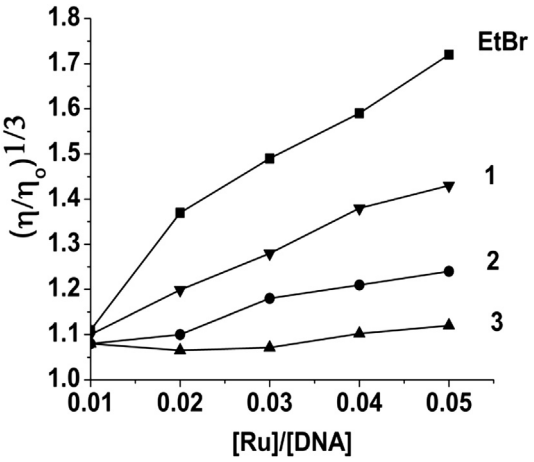

Fig. 10. Effect of increasing amount of ethidium bromide (EtBr), **1**–**3** on relative viscosity of CT-DNA at 30 ± 0.1 °C. The total concentration of DNA is 0.25 mM.

3.10. Molecular docking studies

Molecular docking studies for **1**–**3** were carried out to determine the binding mode with the B-DNA. The relative orientation, interaction, Hydrogen bond and van der Waals interactions in the docked one determined from the results of the docking study. The data were analyzed by using the graphical program Silver Visualizer 1.1. The view shows the different modes of **1** intercalated into the B-DNA sequences (Fig. 13) (for **2** and **3** are given in Supporting information Fig. S8).

For **1**, there are three strong hydrogen bonds between H atom on the intercalative ligand and N atom on a Cytosine of DNA base pairs (N39-DC9:H41, N39-DC9:H42 and H83-DC1:N4). The lengths of these hydrogen bonds (H–O) are 2.479, 2.474 Å and 1.335, **2** and **3** also exhibited three and two hydrogen bonding interactions respectively. The van der Waals interactions (Compound–DNA) for **1** are stronger than **2** and **3** (Table S1). Our calculated results further showed that the intercalative ligand of **1** intercalates into DNA base pairs through major groove, whereas the intercalative ligand of **2** and **3** does through the minor groove. Compound **1** exhibits a strong selectivity for Cytosine only, this complex stabilized by van der Waals interactions through adenine.

This indicated further that DNA-interaction of **1** is stronger than the other compounds. Therefore, based on the viewpoint of hydrogen bond, the trend in DNA-binding affinities, i.e., $K_b(\mathbf{1}) > K_b(\mathbf{2}) > K_b(\mathbf{3})$ can also be explained reasonably. These results are also correlating to the binding constants determined experimentally. The molecular modeling study shows that the compounds accommodates itself easily into the major groove of dsDNA and the compound exhibited a strong selectivity for Adenine and Cytosine.

4. Conclusions

In summary, three mixed-ligand ruthenium(II) polypyridyl compounds **1**–**3** have been synthesized and characterized. Studies of binding ability with CT-DNA suggests that they can bind to DNA in an intercalative mode, in the order of **1** > **2** > **3**. Antiproliferative and cellular uptake studies carried out revealed that all compounds show good cytotoxicity and uptake properties, the difference in efficiencies are due to the intercalating ligand. Therefore we conclude that modification of main ligand can create some interesting differences in the DNA-binding properties and leads to design new complexes with enhanced activity and minimized undesired toxicity.

5. Experimental protocols

5.1. Cellular uptake and flow cytometry

HeLa cells in RPMI medium supplemented with 10% fetal calf serum were seeded in 35 mm tissue culture dishes (Corning) and incubated at 37 °C under a 5% CO_2 atmosphere till 70% confluency. The culture medium was removed and replaced with fresh medium containing the compounds **1**–**3**. After incubation for 1 h, the cell layer was trypsinized and washed twice with cold PBS (phosphate buffered saline). The samples were rinsed in 500 μL of cold PBS and analyzed by a flow cytometer immediately. The samples were collected in FL2 channel (excitation at 488 nm and emission at 585–620 nm). Lymphocytes were isolated from Bovine blood by using Percoll [36,37], were incubated with 50 μM of compound **2** and at different time points from 0 to 4 h, the cells were fixed and mounted on slides for confocal imaging.

5.2. Confocal microscopy

HeLa cells were cultured on cover slips (corning 22 × 50 mm), until they reached 70% confluency. The cells were incubated with **1**–**3** at 50 μM concentration for 2 h, then washed with PBS and photographed with a confocal microscope. The confocal microscope was equipped with an ArKr laser which was used to excite **1**–**3** (488 nm excitation, 600–620 nm emission). Confocal microscopy imaging was carried out on one set without any staining and one set was stained with DAPI (4′,6-diamidino-2-phenylindole, dihydro chloride) (nuclear stain) 0.1 mg mL^{-1} was purchased from Sigma Aldrich, used to identify localization of the compounds and any nuclear disintegration.

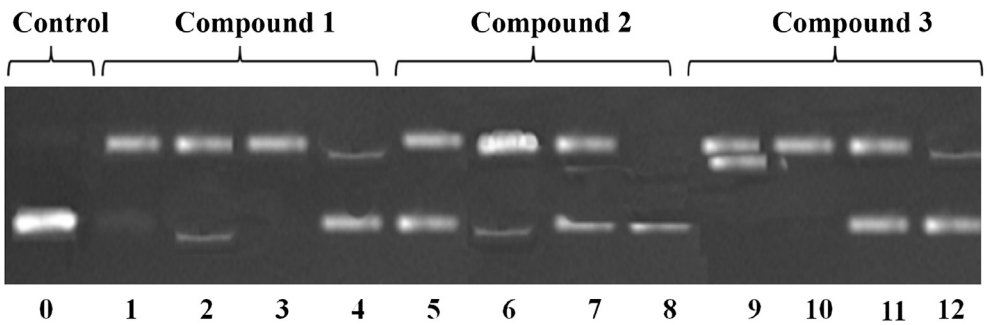

Fig. 11. Photo cleavage of pBR322 DNA in the presence of **1**–**3**, after irradiation with UV light at 365 nm. Lane control is plasmid DNA (unirradiated pBR322), lanes 1–4, 5–8 and 9–12 addition of three compounds of 20, 40, 60 and 80 μM respectively. Lanes 4, 8 and 12 are compounds in presence of Histidine.

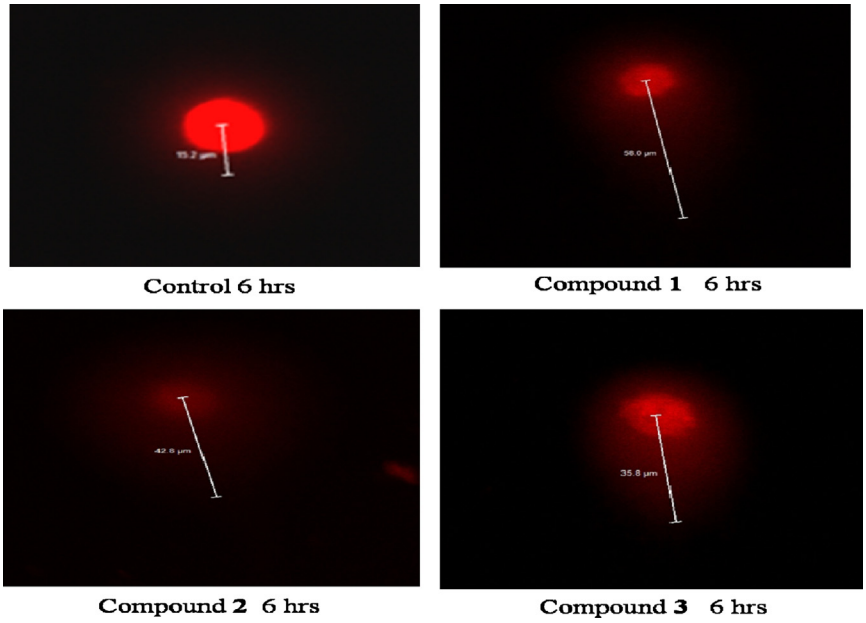

Fig. 12. Confocal microscopy images of HeLa cells treated with 50 μM of **1**–**3** for 6 h and stained by PI.

5.3. Cell viability assay

To study the effects of **1**–**3** on cell growth, selected cell lines growing exponentially were added to 96-well plates at a density of 3×10^3 per well after counting on Bright Line Heamocytometer. To a final volume of 200 μL three compounds **1**–**3** at different concentrations (1–100 μM) were added to cells (final DMSO concentration, 1% v/v). Cell number/proliferation was measured at 48 h using a standard MTT-based assay. Their *in vitro* cytotoxicity was assayed on the basis of the measurement of *in vitro* growth in 96 well plates by cell-mediated reduction of tetrazolium salt to form water insoluble formazan crystals MTT (3-[4,5-dimethylthiazol-2-yl]-2,5-diphenyltetrazolium bromide) cellular viability assay [38]. MTT was added to each well to yield a working concentration of 0.4 mg mL^{-1} and the plates were returned to the incubator for a further 2 h. After this time, the medium was aspirated, 200 μL of DMSO (Sigma Ltd.) was then added to each well and the plates were agitated gently for 5 min before measuring the optical density at 620 nm in each well using Elisa reader. Dose–response curves were plotted for the test compounds and controls after correction by subtracting the background absorbance from that of the blanks. Data were collected for four replicates each and used to calculate the mean. The IC_{50} values (50% inhibitory concentration) were calculated from the plotted absorbance data for the dose–response curves. IC_{50} values (in μM) were expressed as the means ± S.D. Cell lines used for this study were procured from American Type Culture Collection (ATCC), Manassas, VA, USA. Cells were routinely kept in DMEM or RPMI-1640 medium (supplemented with 10% (v/v) fetal

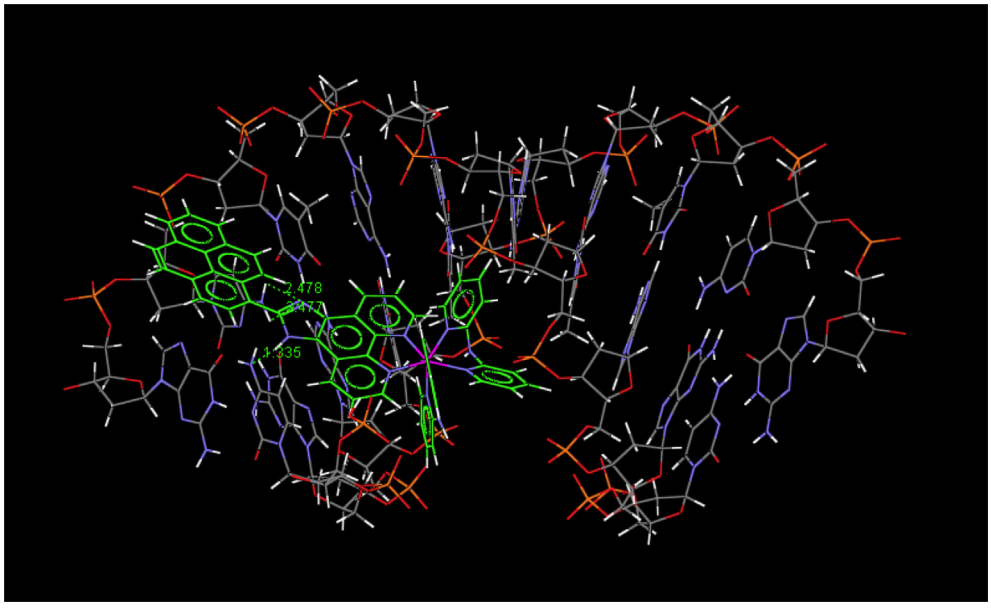

Fig. 13. Hydrogen bonds in DNA-docking model of **1** and B-DNA.

bovine serum (FBS), 2 mM L^{-1} glutamine, 4.5 gL^{-1} glucose, 1× Non-essential amino acids and 1× antibiotics such as penicillin/streptomycin, gentamycin, amphotericin B, nystatin – a basal growth medium). The cell lines were incubated in a humidified atmosphere with 5% CO_2 in air at 37 °C.

5.4. DNA binding studies

Concentrated stock solutions of compounds were prepared by dissolving them in buffer at pH 7.1 in 5% CH_3OH 5 mM Tris–HCl 50 mM NaCl and diluting suitably with corresponding buffer to required concentrations for all the experiments. For absorption and emission interaction of the compounds with CT-DNA was studied in Tris–buffer (5 mM Tris HCl, 50 mM NaCl, pH 7.1). Stock solutions of CT-DNA were prepared in buffer and concentration was determined by UV absorbance by employing an extinction coefficient of 6600 M^{-1} cm^{-1} at 260 nm [39]. The DNA had a ratio of UV absorbance at 260 and 280 nm of about ~1.9:1 indicating that the DNA was sufficiently free of protein [40].

Fluorescence measurements performed at room temperature to determine the binding affinity of the complex with DNA. The titration experiments were performed at ruthenium concentration of 10 μM, to which increments of CT-DNA solution was added until no emission was detected. Steady state emission quenching experiments using varying $[Fe(CN)_6]^{4-}$ as the quencher were performed in absence and presence of DNA. Similar concentrations of DNA and compound were employed to that of emission experiment. $[Fe(CN)_6]^{4-}$ was varied from 0 to 5 μM. Salt dependent studies were conducted in 5 mM Tris–HCl and NaCl concentrations as indicated.

UV–Visible studies were also performed by adopting a procedure analogous to that used for the fluorescence titration experiment. Constant concentration of the compound 3.0 mL (20 μM) was taken in a cuvette to which increments of the DNA stock solution was added until no hypochromism was detected. DNA solution was added reference and sample cuvettes to eliminate the absorbance of DNA itself. The mixture was allowed to equilibrate for 5 min before the spectra was recorded. The intrinsic binding constant K_b of the compound with CT-DNA was evaluated using equation [41].

$$[\mathrm{DNA}]/\left(\varepsilon_a - \varepsilon_f\right) = [\mathrm{DNA}]/\left(\varepsilon_b - \varepsilon_f\right) + 1/K_b\left(\varepsilon_b - \varepsilon_f\right)$$

where ε_a, ε_f and ε_b are the extinction coefficient for apparent, free and bound compound, respectively. A best fit plot of $[DNA]/(\varepsilon_a - \varepsilon_f)$ vs. [DNA] produces a straight line with slope $1/(\varepsilon_b - \varepsilon_f)$ and intercept $1/K_b(\varepsilon_b - \varepsilon_f)$; while K_b is the ratio of slope to intercept.

Viscosity experiments were carried out using BPE-buffer (6 mM Na_2HPO_4, 2 mM NaH_2PO_4, 1 mM Na_2EDTA, pH = 7). Flow time was measured with a digital stopwatch and every sample was tested three times to get an average calculated time. The data were presented as $(\eta/\eta_o)^{1/3}$ vs the concentration of [Ru(II)]/[DNA], where η and η_o are the viscosities of DNA in the presence and absence of compound.

5.5. Photo cleavage

Photo cleavage experiments with DNA were studied by gel-electrophoresis. TAE-buffer (pH 8.0; 40 mM Tris–base, 20 mM acetic acid, 1 mM EDTA) was used for. Supercoiled pBR322 DNA (0.1 μg/μL) was treated with **1**–**3**, and the mixtures were irradiated at 365 nm for 1 h. The samples were then analyzed by 0.8% agarose gel electrophoresis at 50 V for 2 h. The gel was stained with 4 μL (from 1 mg/100 μL) ethidium bromide and photographed under UV light.

5.6. Comet assay

HeLa cells (0.6×10^6 cells/mL) in culture medium were incubated with 50 μM of **1**–**3** for 2, 4 and 6 h at 37 °C. A set of control (untreated) cells were also incubated for similar time. After each time point of treatment 400 μL cells suspension were collected and washed with PBS. 25 μL of each cell suspension were mixed with 200 μL of 1% low melting point agarose, and spread onto microscope slides precoated with 1% normal melting point agarose. Glass cover slips were placed on the drops of agarose, which were allowed to set at 4 °C. Then the cover slips were removed and the cells embedded in agarose were lysed for 16 h by immersion in 2.5 M NaCl, 0.1 M Na_2EDTA, 0.01 M Tris base, pH 10.5, 1% Triton X-100 and 10% DMSO at 4 °C (lysis solution). The slides were then placed in a horizontal gel electrophoresis tank and the DNA was allowed to unwind for 40 min in freshly prepared alkaline electrophoresis solution (0.03 M NaOH and 2 mM Na_2EDTA, pH > 13). Electrophoresis was carried out in the alkaline solution for 30 min at 0.6 V/cm and approximately 42 mA at 4 °C. The slides were washed in chilled distilled water for 10 min to neutralize the excess alkali. The gels were air-dried for 30 min and were stained with 200 μL of PI (Propidium Iodide, 10 μg/mL) for another 20 min. The gels were destained with chilled distilled water, air-dried and scored for comets by confocal microscopic analysis. A total of 20 comets on each gel were scored and the average tail length measured with Leica confocal microscopy software.

5.7. Docking simulations

The molecular docking calculations for all three were done using the 3.01 GOLD (Genetic Optimization for Ligand Docking) program, which was based on Genetic Algorithms. This method allows partial flexibility of the hydroxyl groups of the respective DNA molecule and full flexibility of the ligand. The DNA sequences used for the docking simulations were obtained from the PDB protein data banks, and are associated with ligands. Using Discovery Studio 3.0, we built ((C-G-A-T-T-A-A-T-C-G) and the PDB code: 1D49) initio double helix DNA decamer. The DNA structures were chosen as to allow an evaluation of the binding preference for CG sequences. In order to evaluate the GOLD scoring function, water molecules were removed from the DNA molecules.

Acknowledgments

Council of Scientific and Industrial Research (CSIR, New Delhi, India), is greatfully acknowledged for the financial support in the form of Junior Research Fellow to Dr. C. Shobha Devi. Authors are also thankful to Department of Biotechnology (DBT) ISLARE, Osmania University.

Appendix A. Supplementary data

Supplementary data related to this article can be found at http://dx.doi.org/10.1016/j.ejmech.2013.11.005

References

[1] K.E. Erkkila, D.T. Odem, J.K. Barton, Chem. Rev. 99 (1999) 2777–2796.
[2] C. Metcalfe, J.A. Thomas, Chem. Soc. Rev. 32 (2003) 215–224.
[3] Y. Xiong, L.N. Ji, Coord. Chem. Rev. 185 (1999) 711–733.
[4] R. Blasius, C. Moucheron, A.K. Mesmasker, Eur. J. Inorg. Chem. 20 (2004) 3971–3979.
[5] L.N. Ji, Z. Xiao-Hua, L. Jin-Gang, Coord. Chem. Rev. 216 (2001) 513–536.
[6] G.Z. Chang, L.M. Chunn, W.Y. Xiao, L.Q. Qian, S. Yang, K. Jun, X. Yan, Chem. Biodivers. 8 (2011) 1486–1496.
[7] J. Liu, W. Zheng, S. Shi, C. Tan, J. Chen, K. Zheng, L.N. Ji, J. Inorg. Biochem. 102 (2008) 193–202.

[8] C.S. Devi, D.A. Kumar, S.S. Singh, N. Gabra, N. Deepika, Y.P. Kumar, S. Satyanarayana, Eur. J. Med. Chem. 64 (2013) 410–421.
[9] D.R. Boer, A. Canals, M. Coll, Dalton Trans. (2009) 399–414.
[10] S.M. Haider, S. Neidle, G.N. Parkinson, Biochimie 93 (2011) 1239–1251.
[11] R. Martin Gill, T.A. . Jim, Chem. Soc. Rev. 41 (2012) 3179–3192.
[12] T. Caiping, W. Shouhai, L. Sensen, W. Minxu, C. Yu, Z. Lingjun, Z. Yiping, L. Wu, P. Wenlie, L.N. Ji, Dalton Trans. 40 (2011) 8611–8621.
[13] H.L. Huang, Z.Z. Li, Z.H. Liang, Y.J. Liu, Eur. J. Inorg. Chem. (2011) 5538–5547.
[14] J.L. Yun, H.L. Zhen, L.H. Xian, Z.Z. Li, H.Y. Jun, L.H. Hong, Inorg. Chim. Acta 387 (2012) 117–124.
[15] C.S. Devi, S. Satyanarayana, J. Coord. Chem. 65 (2012) 474–486.
[16] C.S. Devi, P. Nagababu, M. Shilpa, K.Y. Praveen, R.M. Rajender, M.G. Nazar, S. Satyanarayana, J. Iran. Chem. Soc. 9 (2012) 671–680.
[17] K.Y. Praveen, M. Shilpa, P. Nagababu, R.M. Rajender, K.L. Reddy, M.G. Nazar, S. Satyanarayana, J. Fluoresc. 3 (2012) 835–847.
[18] P. Nagababu, M. Shilpa, L.L.J. Naveena, I. Bhatnagar, P.N.B.S. Srinivas, K.Y. Praveen, K.L. Reddy, S. Satyanarayana, J. Fluoresc. 21 (2011) 563–572.
[19] M. Shilpa, L.L.J. Naveena, D. Gayatri, A. Nagarjuna, K.Y. Praveen, P. Nagababu, S. Satyanarayana, J. Inclusion Phenom. Macrocyclic Chem. 70 (2011) 187–195.
[20] E.A. Steck, A.R. Day, J. Am. Chem. Soc. 65 (1943) 452–456.
[21] R.L. Blakley, M.K. DeArmond, J. Am. Chem. Soc. 109 (1987) 4895–4901.
[22] K.K. Lo, T.K. Lee, J.S. Lau, W.L. Poon, S.H. Cheng, Inorg. Chem. 47 (2008) 200–208.
[23] C.A. Puckett, J.K. Barton, Biochemistry 47 (2008) 11711–11716.
[24] C.A. Puckett, J.K. Barton, J. Am. Chem. Soc. 129 (2007) 46–47.
[25] T. Caiping, L. Sensen, W. Shouhai, H. Sheng, Z. Lingjun, C. Yu, W. Minxu, Z. Yiping, L. Wu, P. Wenlie, L.N. Ji, X. Anlong, J. Med. Chem. 53 (2010) 7613–7624.
[26] J.Y. Hui, C. Yu, Y. Lin, H. Zhi-feng, Z. Li-hya, Eur. J. Med. Chem. 55 (2012) 146–154.
[27] P. Vanessa, J. Tanmaya, L. Anna, M. Cristina, S. Julia, O. Ingo, S. Leone, F. Stefano, G. Gilles, J. Am. Chem. Soc. 134 (2012) 20376–20387.
[28] C. Riccardi, I. Nicoletti, Nat. Protoc. 1 (2006) 1458–1461.
[29] I. Vermes, C. Haanen, H. Steffens-Nakken, C. Reutelingsperger, J. Immunol. Methods 184 (1995) 39–51.
[30] R. Venugopal, M. Mariappan, S. Eringathodi, P. Mallayan, S.P. Vaiyapuri, A.A. Mohammad, Dalton Trans. (2008) 2157–2170.
[31] J.R. Lakowicz, G. Webber, Biochemistry 12 (1973) 4161–4170.
[32] M. Mariappan, M.G. Bhaskar, Eur. J. Inorg. Chem. (2005) 2164–2173.
[33] S. Satyanarayana, J.C. Dabrowiak, J.B. Chaires, Biochemistry 31 (1992) 9319–9324.
[34] J.K. Barton, A.L. Raphael, J. Am. Chem. Soc. 106 (1984) 2466–2468.
[35] B. Armitage, Chem. Rev. 98 (1998) 1171–1200.
[36] P.L. Olive, J.P. Banath, Nat. Protoc. 1 (2006) 23–29.
[37] D. Stibenz, C. Buhrer, J. Immunol. 39 (1994) 59–63.
[38] V. Pistoia, C. Anna, B. Lucia, Z. Simona, D. Mariella, F. Manlio, Stem Cells 11 (1993) 150–155.
[39] J. Marmur, J. Mol. Biol. 3 (1961) 208–218.
[40] M.E. Reichmann, S.A. Rice, C.A. Thomas, P. Doty, J. Am. Chem. Soc. 76 (1954) 3047–3053.
[41] A. Wolfe, G.H. Shimer, T. Mechan, Biochemistry 26 (1987) 6392–6396.

Further reading

[42] A.P. Silverman, E.T. Kool, Chem. Rev. 106 (2006) 3775–3789.
[43] R. Martínez, L. Chacón-García, Curr. Med. Chem. 12 (2005) 127–151.
[44] J.C. Tan, B. Wang, L. Zhu, Bioorg. Med. Chem. 17 (2009) 614–620.